PHYSICAL REVIEW B

SOLID STATE

THIRD SERIES, VOL. 8, NO. 8 15 OCTOBER 1973

Lattice Dynamics of Gold*

J. W. Lynn†, H. G. Smith, and R. M. Nicklow

Solid State Division, Oak Ridge National Laboratory, Oak Ridge, Tennessee 37830

(Received 3 May 1973)

The complete phonon dispersion relations for gold in the high-symmetry directions have been measured at room temperature by the coherent inelastic scattering of neutrons. It is found that the forces in gold are not homologous with the other noble metals, the frequencies of gold lying appreciably higher than those "scaled" from copper and silver. An analysis of the data in terms of different force-constant models reveals that a general tensor force is required for the first-neighbor interaction, whereas for neighbors beyond the first either general tensor or axially symmetric forces give an excellent fit to the data. The axially symmetric model alone does not adequately describe the data even when forces extending to ninth-nearest neighbors are included in the fit. In addition, simple screened-pseudopoential models were fit to the data and these results also indicate the need for the first-neighbor interaction to be general. Frequency distribution functions and related thermodynamic quantities were calculated from the various force-constant models. The Debye temperature Θ_C versus temperature curves obtained show an anomaly at low temperatures consistent with the $\Theta_C(T)$ obtained from specific-heat measurements. The relation between this anomaly and the character of the dispersion curves is given.

INTRODUCTION

Noble metals have been the subject of extensive experimental and theoretical investigations for many years. The electronic properties, including the Fermi surface, have been investigated by photoemission, resistivity, specific-heat, and de Haas–van Alphen measurements, for example, and the mechanical properties by ultrasonic and other types of measurements. The phonon spectrum, of course, is related to these properties through the forces existing in the solid. It is the goal of the above experiments, as well as the present one, to elucidate as much as possible the nature of these forces.

From the point of view of lattice dynamics, the noble metals are particularly interesting since they are monovalent metals which form simple face-centered-cubic structures, and large, pure, single crystals are readily available. They also are well suited to investigations of the effects of impurities on their phonon spectra and thermodynamic properties, since they readily accept a variety of substitutional impurities over broad concentration ranges, and their simple structures should facilitate comparison between theory and experiment.[1] In order to determine the effects of impurities, of course, a detailed investigation of the pure host material must first be made. The lattice dynamics of copper have been studied exhaustively both at room temperature[2–4] and low temperature.[4] More recently, silver has been investigated,[5,6] although its rather large absorption cross section for thermal neutrons (~65 b) increased the difficulty of the experiment. The force systems of copper and silver were found to be approximately homologous[5]; that is, the forces have the same form relative to their respective lattices. However, deviations from this simple behavior might be expected for gold since the temperature[7] and pressure[8] dependences of the elastic constants indicate that noncentral many-body forces are of rapidly increasing importance in the series Cu, Ag, and Au. Furthermore, measurements of the specific heat of gold[9] show an anomalous Debye temperature $\Theta_C(T)$ at low temperatures. The lattice dynamics of gold, with its large neutron absorption cross section (~100 b) and heavy mass, have not been investigated

in detail until now.

EXPERIMENTAL APPARATUS AND RESULTS

The sample was a single crystal in the form of a cylinder, 0.5 in. in diameter and 1.5 in. long, which was commercially purchased and quoted as 99.999% pure. The crystal had a mosaic spread $<0.1°$, and the [001] crystallographic direction was along the cylinder axis. The measurements were made at room temperature (296 °K) on two triple-axis spectrometers located at the High Flux Isotope Reactor. The majority of the data was obtained under neutron-energy-loss conditions with the "constant-Q" method of operation, although the "constant-E" method was also used on the longitudinal branches at small wave vectors. On the HB-4A spectrometer, neutrons with fixed energies of 7.898 or 9.516 THz were incident on the sample. The flight path from the monochromator to the sample is ~7 m, giving a vertical and horizontal angular divergence of ~0.25°. No additional collimation was used before the sample. For most of the measurements on this unit the horizontal collimation after the sample was 0.67° and the analyzer was a zinc crystal with the (0002) planes oriented for reflection, Zn (0002). The HB-3 spectrometer, described in detail elsewhere,[10] was used with 0.67° horizontal collimation both before and after the sample and a Be (0002) analyzer set to scatter neutrons with energies of 6.0 or 8.0 THz. Both spectrometers used Be (0002) crystals as monochromators.

The effects due to finite instrumental resolution on the frequencies at small wave vectors, where the percentage shifts in frequency are usually largest, were systematically investigated on the HB-4A spectrometer. Detailed measurements of the L[00ζ], T[00ζ], L[$\zeta\zeta$0], and T$_1$[$\zeta\zeta$0] modes were made with progressively better resolution until the effects of changing the resolution became negligible. The best resolution used was obtained with 0.33° horizontal collimation after the sample and 1.0° vertical and horizontal collimation after a Be $(10\bar{1}1)$ analyzer. The shifts in the longitudinal frequencies were smaller than the experimental errors involved. The T[00ζ] frequencies were shifted to lower frequencies by no more than 3% and merged with the low resolution measurements for $\zeta \geq 0.25$. The T$_1$[$\zeta\zeta$0] branch, as expected, was the most seriously affected, the frequencies shifting downwards as much as 13%. For $\zeta \geq 0.35$ the effects of changing the resolution were negligible for this branch as well. It should be pointed out that the measurements at the smallest wave vectors, owing to the Bragg peak at Γ, could be accurately made only with the better resolution.

The results of the measurements for the four high-symmetry directions [00ζ], [$\zeta\zeta$0], [$\zeta\zeta\zeta$], and [10ζ] are given in Table I and are illustrated in Fig. 1. The group-theory notation is that of Koster,[11] ν is in units of THz, and ζ is the reduced wave vector ($\zeta = aq/2\pi$, where q is a component of the phonon wave vector). The errors are determined from the reproducibility of the results measured around different reciprocal-lattice points and with the two different spectrometers, and are considered to be no greater than one standard deviation. No corrections have been made for effects due to the finite resolution of the instrument or absorption of the sample. In all, 240 usable neutron

TABLE I. Normal-mode frequencies for the symmetry branches in gold. Frequency units are THz.

L[00ζ]		T[00ζ]		L[$\zeta\zeta$0]	
ζ	ν	ζ	ν	ζ	ν
0.052	0.50 ± 0.07	0.10	0.41 ± 0.04	0.058	0.75 ± 0.08
0.092	0.75 ± 0.06	0.15	0.58 ± 0.03	0.074	1.00 ± 0.07
0.116	1.00 ± 0.05	0.20	0.75 ± 0.03	0.109	1.25 ± 0.08
0.179	1.50 ± 0.05	0.25	0.91 ± 0.03	0.12	1.50 ± 0.10
0.206	1.65 ± 0.04	0.30	1.09 ± 0.03	0.17	2.00 ± 0.08
0.293	2.25 ± 0.04	0.40	1.46 ± 0.03	0.201	2.40 ± 0.06
0.30	2.32 ± 0.04	0.50	1.84 ± 0.03	0.28	3.00 ± 0.05
0.40	2.85 ± 0.06	0.60	2.16 ± 0.03	0.35	3.50 ± 0.05
0.47	3.30 ± 0.08	0.70	2.41 ± 0.04	0.45	3.85 ± 0.10
0.552	3.70 ± 0.08	0.80	2.61 ± 0.05	0.50	3.96 ± 0.06
0.60	3.88 ± 0.06	0.90	2.73 ± 0.05	0.60	3.84 ± 0.05
0.70	4.17 ± 0.06	1.00	2.75 ± 0.04	0.66	3.70 ± 0.05
0.80	4.40 ± 0.06			0.70	3.55 ± 0.06
0.90	4.58 ± 0.06			0.75	3.34 ± 0.05
1.00	4.61 ± 0.05			0.80	3.15 ± 0.05
				0.90	2.83 ± 0.05
				1.00	2.75 ± 0.04

T$_1$[$\zeta\zeta$0][a]		T$_2$[$\zeta\zeta$0][a]		L[$\zeta\zeta\zeta$]	
ζ	ν	ζ	ν	ζ	ν
0.10	0.31 ± 0.02	0.10	0.56 ± 0.03	0.035	0.60 ± 0.08
0.15	0.48 ± 0.02	0.20	1.10 ± 0.03	0.06	1.00 ± 0.08
0.20	0.63 ± 0.04	0.30	1.63 ± 0.04	0.12	1.80 ± 0.09
0.25	0.83 ± 0.03	0.40	2.15 ± 0.05	0.176	2.40 ± 0.10
0.30	1.02 ± 0.03	0.50	2.71 ± 0.05	0.23	3.00 ± 0.15
0.35	1.23 ± 0.03	0.60	3.25 ± 0.05	0.26	3.40 ± 0.15
0.40	1.44 ± 0.03	0.70	3.77 ± 0.07	0.30	3.75 ± 0.06
0.45	1.64 ± 0.05	0.80	4.26 ± 0.07	0.35	4.14 ± 0.06
0.50	1.79 ± 0.04	0.90	4.53 ± 0.07	0.40	4.45 ± 0.05
0.55	1.96 ± 0.05	1.00	4.61 ± 0.05	0.45	4.64 ± 0.05
0.60	2.08 ± 0.05			0.50	4.70 ± 0.04
0.65	2.18 ± 0.05				
0.70	2.34 ± 0.05				
0.75	2.43 ± 0.05				
0.80	2.55 ± 0.08				
0.90	2.70 ± 0.06				
0.95	2.74 ± 0.06				
1.00	2.75 ± 0.04				

T[$\zeta\zeta\zeta$]		π[10ζ]		Λ[10ζ]	
ζ	ν	ζ	ν	ζ	ν
0.10	0.51 ± 0.03	0.00	4.61 ± 0.05	0.00	2.75 ± 0.04
0.15	0.76 ± 0.03	0.10	4.57 ± 0.05	0.10	2.74 ± 0.05
0.20	1.00 ± 0.02	0.20	4.46 ± 0.05	0.20	2.73 ± 0.05
0.25	1.23 ± 0.02	0.30	4.23 ± 0.05	0.30	2.70 ± 0.04
0.30	1.44 ± 0.02	0.40	3.92 ± 0.05	0.40	2.63 ± 0.03
0.35	1.63 ± 0.03	0.50	3.63 ± 0.05	0.50	2.63 ± 0.03
0.40	1.74 ± 0.03	0.60	3.30 ± 0.05	0.60	2.64 ± 0.03
0.45	1.85 ± 0.04	0.70	3.06 ± 0.06	0.70	2.69 ± 0.04
0.50	1.86 ± 0.04	0.80	2.90 ± 0.07	0.80	2.73 ± 0.05
		0.90	2.80 ± 0.07	0.90	2.74 ± 0.05
		1.00	2.75 ± 0.04	1.00	2.75 ± 0.04

[a]The polarization vectors for the T$_1$ and T$_2$[$\zeta\zeta$0] branches are parallel to [$\bar{\zeta}\zeta$0] and [00ζ], respectively.

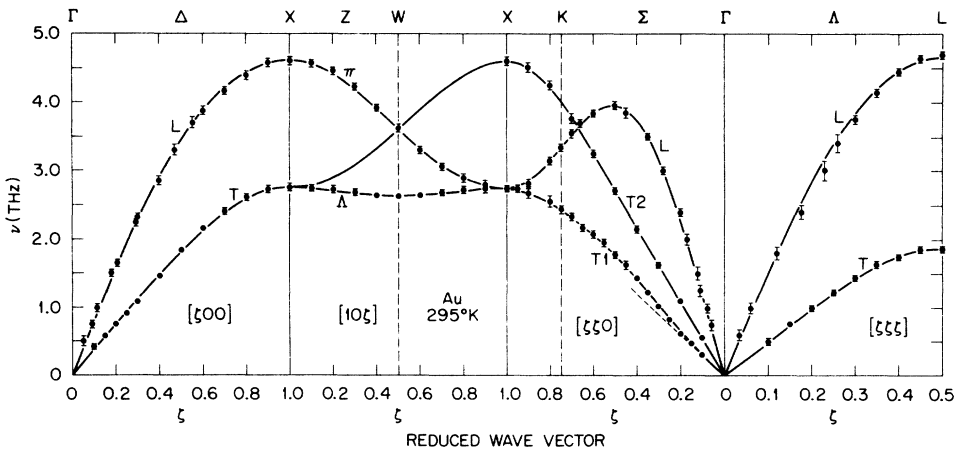

FIG. 1. Room-temperature phonon dispersion relations for gold in the principal symmetry directions. The solid curves represent both the fourth-neighbor general force model (M1) and the fifth-neighbor mixed axially symmetric model (M2). The dotted line in the Σ direction is the velocity of sound appropriate to the $T_1[\zeta\zeta 0]$ branch. The reduced wave vector $\zeta = aq/2\pi$.

groups were measured. Each group was fit by a least-squares procedure to a Gaussian distribution plus sloping background. Several typical groups are shown in Fig. 2.

A comparison of the zone-boundary phonon frequencies of gold with those scaled from the other noble metals has been made in Table II. If the forces are homologous then the relationship

$$\nu(\mathrm{Au}) = \nu(\mathrm{Cu;\ Ag}) \left\{ \frac{Ma^2(\mathrm{Cu;\ Ag})}{Ma^2(\mathrm{Au})} \right\}^{1/2}$$

should hold. It is evident that the frequencies of gold lie appreciably above those expected from scaling, and the relative splitting of the transverse and longitudinal branches is greater than in either copper or silver.

The frequencies measured at small wave vectors are in good agreement with the frequencies calculated from the measured elastic constants (velocity of sound lines). In general as one proceeds further into the zone the measured frequencies drop below these lines (negative dispersion). A notable exception to this is the $T_1[\zeta\zeta 0]$ branch in gold. The small-wave-vector (high-resolution) measurements fall, within experimental error, on the velocity-of-sound line, but as ζ increases the phonon dispersion curve rises above the velocity of sound (positive dispersion). Even at the zone boundary (K point) the dispersion curve lies well above this line. Similar effects have been observed for this branch in other face-centered-cubic metals, for example, palladium,[12] platinum,[13] and to a smaller extent, copper.[2]

FORCE MODEL AND PSEUDOPOTENTIAL CALCULATIONS

The dispersion relations were fit by a least-squares procedure to Born–von Kármán atomic force constant models in which the forces were assumed to be general tensor, axially symmetric (AS), or a mixture of general tensor and axially symmetric.[14] The elastic constants were included in the calculations as independent data. In general the models which fit the neutron data well were also in good agreement with the measured elastic constants.[7]

For copper Nicklow *et al.*[4] found that the AS model gave a significantly better fit to their data (high-symmetry-direction data only) than did the general model with the same number of adjustable

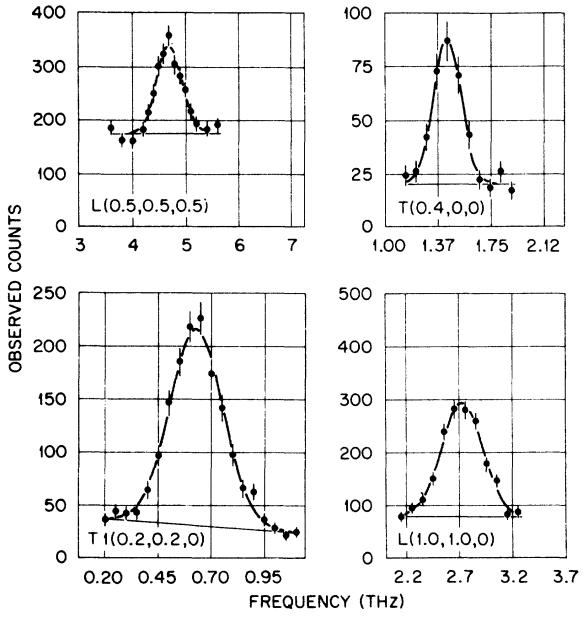

FIG. 2. Several typical "constant-Q" phonon scans. The solid curves are the computer least-squares fits.

TABLE II. Comparison of the zone-boundary frequencies scaled from Cu and Ag with those measured in Au. Frequency units are THz.

Zone-boundary point	ν_{scaled}	ν_{Au}
X	3.65	4.61
	2.58	2.75
L	3.68	4.70
	1.72	1.86

force constants. Furthermore, the general-tensor force constants for silver[5] satisfy, within experimental error, the conditions for axial symmetry. This is to be expected since the forces in silver were found to be approximately homologous to those in copper. In contrast to this, the AS model did not give a good fit to the gold dispersion relations even when forces extending to ninth nearest neighbors were included. On the other hand, both a fourth-neighbor general force model (M1) with twelve parameters, and a fifth-neighbor mixed model (M2) with the nearest-neighbor interaction general and the remaining forces axially symmetric (11 parameters), gave excellent fits to the data. In fact, the general model with first-neighbor interactions alone (three parameters) fit the data to within 5%. Thus, in order to explain the data a general first-neighbor interaction is required. This is consistent with the interpretation of the temperature[7] and pressure[8] dependences of the elastic constants. The fit did not significantly improve by extending the M2 model to further than fifth nearest neighbors; the general force model cannot be extended beyond the fourth nearest neighbors if the force constants are to be determined from high-symmetry data alone.

The force constants resulting from the fitting procedure are given in Table III for the M1 and M2 models. The force-constant notation is that of Squires,[15] and the force constants are in units of 10^3 dyn/cm. The errors quoted are least-squares statistical errors. In Fig. 1 the M1 and M2 models, both represented by the solid lines, are compared with the data. The over-all fit is excellent.

The conclusions reached by the Born–von Kármán analysis were substantiated by calculations with very simple screened-pseudopotential models.[16,17] Simplified (l-independent) Heine–Abarenkov and Lin–Kleinman pseudopotentials,[18–20] with free-electron RPA screening, were also used to fit the data. The screened-pseudopotential forces are axially symmetric for these two models. Although quantitative agreement cannot be expected for these oversimplified models, some interesting results were nevertheless obtained. With the ionic charge Z fixed at unity, the calculated spectra fell well below the observed frequencies. Interestingly enough, however, the $T_1[\zeta\zeta 0]$ branch did exhibit positive dispersion, which was produced by the screening contributions to the dynamical matrix. When Z was allowed to vary, considerably better fits could be obtained for most of the spectrum. However, these "best fits" (typically with values of $Z \sim 1.5$) displayed an extreme version of the positive dispersion observed in the $T_1[\zeta\zeta 0]$ branch. Generally, in all these calculations the longitudinal modes were fit better than the transverse modes. By including in the calculations general first-neighbor Born–von Kármán force constants to simulate the repulsive forces omitted[21] in the pseudopotential models, much better fits to all modes were possible. The results, however, were not as good as those of the M1 or M2 models.

FREQUENCY DISTRIBUTION FUNCTIONS AND THERMODYNAMIC QUANTITIES

From the various force-constant models we have computed the frequency distribution functions $g(\nu)$ using the method developed by Gilat and Raubenheimer.[22] The $g(\nu)$ distributions calculated from the M1 and M2 models are shown in Fig. 3. For comparison the $g(\nu)$ distribution for copper, after Nicklow *et al.*,[4] and for silver, which we calculated from the fourth-neighbor general force constants given by Kamitakahara and Brockhouse,[5] are also shown. The shapes of the spectra for copper and silver are quite similar. This is to be expected

TABLE III. Best-fit force constants for general (M1) and mixed axially symmetric models (M2).

Neighbors and location		Force constants (10^3 dyn/cm) M1		M2		Restrictions for the M2 model
1 (1,1,0)	α_1^1	16.43	± 0.09	16.61	± 0.10	
	α_2^1	−6.54	± 0.10	−6.65	± 0.15	
	β_3^1	19.93	± 0.14	19.93	± 0.16	
2 (2,0,0)	α_1^2	4.04	± 0.17	3.95	± 0.22	
	α_2^2	−1.27	± 0.11	−1.13	± 0.12	
3 (2,1,1)	α_1^3	0.80	± 0.05	1.00	± 0.05	
	α_2^3	0.39	± 0.05	0.28	± 0.04	
	β_1^3	0.16	± 0.06	0.24		$\beta_1^3 = \frac{1}{3}(\alpha_1^3 - \alpha_2^3)$
	β_2^3	0.54	± 0.04	0.48		$\beta_2^3 = 2\beta_1^3$
4 (2,2,0)	α_1^4	−0.75	± 0.05	−0.57	± 0.05	
	α_3^4	−0.14	± 0.09	−0.21	± 0.07	
	β_3^4	−0.36	± 0.11	−0.36		$\beta_3^4 = \alpha_1^4 - \alpha_3^4$
5 (3,1,0)	α_1^5			−0.17	± 0.06	
	α_2^5			−0.02	± 0.03	
	α_3^5			0.00		$\alpha_3^5 = \frac{1}{8}(9\alpha_2^5 - \alpha_1^5)$
	β_3^5			−0.06		$\beta_3^5 = \frac{3}{8}(\alpha_1^5 - \alpha_2^5)$

Force-constant matrix $\begin{pmatrix} \alpha_1^n & \beta_3^n & \beta_2^n \\ \beta_3^n & \alpha_2^n & \beta_1^n \\ \beta_2^n & \beta_1^n & \alpha_3^n \end{pmatrix}$

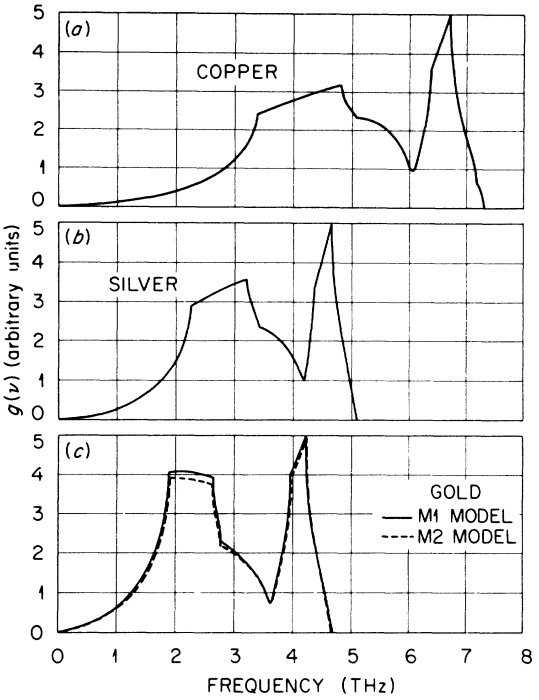

FIG. 3. Room-temperature frequency distribution functions (a) for copper, after Nicklow *et al.* (Ref. 4) using the axially symmetric model; (b) for silver, calculated from the fourth-neighbor general force constants determined by Kamitakahara and Brockhouse (Ref. 5); (c) for gold, calculated from the fourth-neighbor general (M1) model (solid curve) and the fifth-neighbor mixed axially symmetric (M2) model (dotted curve).

since they were found to be approximately homologous. The $g(\nu)$ for gold departs from this similarity.

From these frequency distributions the Debye temperatures Θ_C and Θ_M, related to the specific heat and Debye-Waller factor, respectively, have been calculated as a function of temperature. Previous investigations on copper[4] and aluminum[23] indicate that when the phonon dispersion curves are measured at a temperature low enough so that anharmonic effects are negligible, quantitative agreement is obtained between thermodynamic measurements and the low-temperature properties calculated from the measured dispersion relations, and that the general effect of anharmonicity[24] is to lower the calculated $\Theta_C(T)$ approximately uniformly. In Fig. 4 the $\Theta_C(T)$ calculated from the M1 model is compared with the $\Theta_C(T)$ obtained from specific-heat measurements.[9,25-27] The $\Theta_C(T)$ for the M2 model lies within 0.5 °K of the M1 model for all temperatures. It is clear that anharmonic effects are important in gold at room temperature. Nevertheless the qualitative agreement is very good.

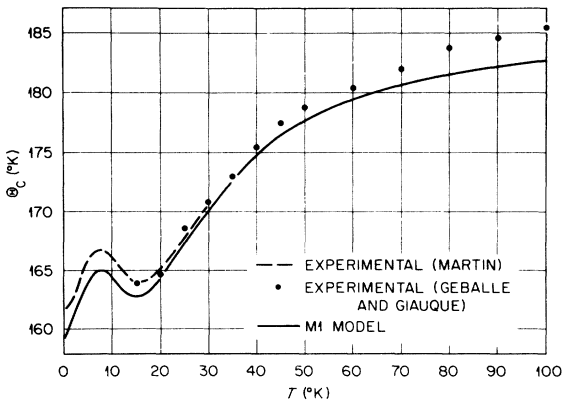

FIG. 4. Debye temperature $\Theta_C(T)$ calculated from the fourth-neighbor general (M1) model (solid curve) compared with the $\Theta_C(T)$ obtained from specific-heat measurements (Refs. 9 and 25).

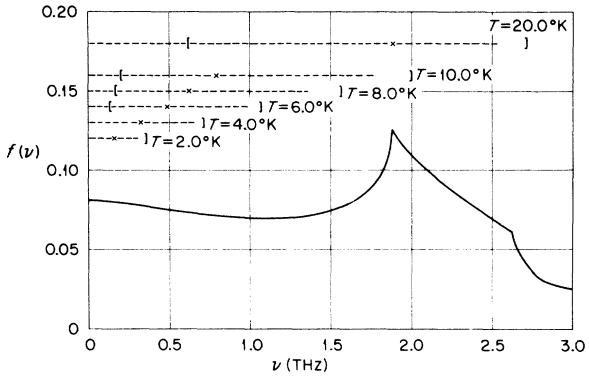

FIG. 5. $f(\nu)=g(\nu)/\nu^2$ calculated from the fourth-neighbor general force model (M1) along with an indication of the regions in frequency which contribute to C_V for different temperatures (see text).

The initial rise in $\Theta_C(T)$ as the temperature increases from 0 °K is particularly noteworthy. All the force models tried, including the pure-AS model, produced this initial rise. In calculating the frequency distribution function one expects[28] that if at some frequency the slope of one of the branches increases above the velocity of sound (positive dispersion), its contribution to $g(\nu)$ is reduced. Hence (all else being equal) $\Theta_C(T)$ would increase if T moves into a range where this frequency region gives the dominant contribution to $\Theta_C(T)$. Indeed, this is just the behavior found. Figure 5 shows the low-frequency portion of $f(\nu)=g(\nu)/\nu^2$ as a function of ν for gold. In the Debye theory $g(\nu)\sim\nu^2$, so that $f(\nu)$ is just a constant. For real crystals this behavior is, of course, only observed near $\nu=0$, and the plot of $f(\nu)$ then illustrates the deviations from this simple behavior. The effect of positive dispersion is to decrease $f(\nu)$, and negative dispersion to increase it. For most "normal" materials, for

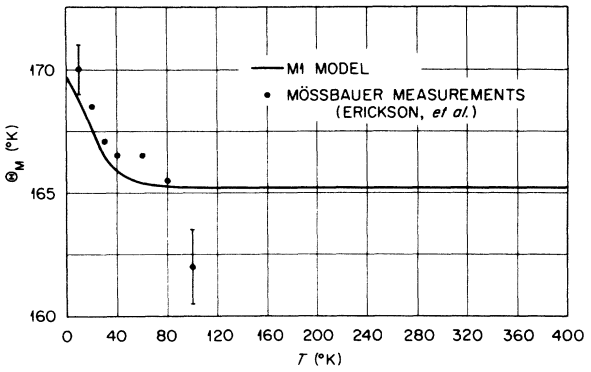

FIG. 6. Comparison of the $\Theta_M(T)$ obtained from the M1 force model with the Mössbauer measurements of Erickson *et al.* (Ref. 32).

example nickel,[29] $f(\nu)$ is constant until the lowest-frequency transverse branch begins to "bend over" (negative dispersion). This gives a rapid rise in $f(\nu)$ up to the first critical point, and hence a characteristic decrease in $\Theta_C(T)$. For gold, however, $f(\nu)$ first drops below $f(0)$, and hence $\Theta_C(T)$ first increases.

The contributions to the specific heat C_V [from which $\Theta_C(T)$ is calculated] as a function of ν for different temperatures are also shown in Fig. 5. For each temperature the x labels the frequency at which the maximum contribution to C_V occurs and the brackets indicate where the contribution has dropped off to 20% of the maximum. The end of the dotted line indicates the frequency ν_{max} up to which 90% of the total contribution to C_V is obtained. It is clearly seen that at 8 °K, where the peak in $\Theta_C(T)$ occurs, the main contribution to C_V comes from the region where $f(\nu)$ falls below the Debye value $f(0)$. Note that $h\nu_{max} \gg kT$, and that the range of frequencies contributing to C_V rapidly expands as T increases. Hence, if the positive dispersion does not occur at low enough frequencies, there will be no T for which this frequency region dominates C_V, and the effect will be washed out. In gold, for example, when $T > \sim 50$ °K there is no frequency at which the contribution to C_V drops below 20% of the maximum.

To further check the source of this behavior, we refit the general-force-constant model to the data, but with the low-frequency ($\zeta \leq 0.5$) portion of the $T_1[\zeta\zeta 0]$ branch modified to fit on a straight line. The initial rise in the resulting $\Theta_C(T)$ was absent. The $f(\nu)$ for aluminum,[30] whose $\Theta_C(T)$ shows an analogous rise at low temperatures, both in the specific-heat measurements[31] and in the neutron data analysis,[23] also first drops below $f(0)$ before peaking at the first critical point. The $T_2[\zeta\zeta 0]$ branch in aluminum shows positive dispersion.

In Fig. 6 the effective Debye temperature $\Theta_M(T)$ appropriate to Mössbauer recoilless fraction and x-ray or neutron Bragg intensity measurements is plotted for the M1 model. The $\Theta_M(T)$ for the M2 model lies ~0.25 °K above the M1 model for all temperatures. The experimental points are from Mössbauer measurements reported by Erickson *et al.*[32] using an internal-conversion coefficient of $\alpha = 4.30$. There are several determinations of $\Theta_M(T = 296$ °K) from x-ray data,[33] but the results range from 160 to 188 °K and hence are not shown in the figure.

SUMMARY

The high-symmetry phonon dispersion relations for gold have been measured at room temperature. A comparison with the other noble metals shows that the frequencies of gold do not scale with those of Cu or Ag. Analyses of the data in terms of both atomic-force-constant and screened-pseudopotential models indicate that core-core and/or noncentral nearest-neighbor interactions are important. Frequency distribution functions and the Debye temperatures $\Theta_C(T)$ and $\Theta_M(T)$ were calculated from the force-constant models and the calculated $\Theta_C(T)$ have an anomaly at low temperatures consistent with specific-heat measurements. This anomaly is found to be directly related to the positive dispersion observed in the $T_1[\zeta\zeta 0]$ branch.

ACKNOWLEDGMENTS

The authors would like to thank Dr. M. Mostoller for making his pseudopotential programs available to us and assisting in those calculations. We would also like to acknowledge helpful discussions with Dr. N. Wakabayashi and valuable technical assistance provided by J. L. Sellers.

---

*Research sponsored by the U. S. Atomic Energy Commission under contract with the Union Carbide Corporation.

†Oak Ridge Associated Universities Graduate Fellow from the Georgia Institute of Technology.

[1]E. C. Svensson and W. A. Kamitakahara, Can. J. Phys. **49**, 2291 (1971).

[2]E. C. Svensson, B. N. Brockhouse, and J. M. Rowe, Phys. Rev. **155**, 619 (1967), and references therein.

[3]S. K. Sinha, Phys. Rev. **143**, 422 (1966).

[4]R. M. Nicklow, G. Gilat, H. G. Smith, L. J. Raubenheimer, and M. K. Wilkinson, Phys. Rev. **164**, 922 (1967).

[5]W. A. Kamitakahara and B. N. Brockhouse, Phys. Lett. A **29**, 639 (1969).

[6]W. Drexel, W. Gläser, and F. Gompf, Phys. Lett. A **28**, 531 (1969).

[7]J. R. Neighbours and G. A. Alers, Phys. Rev. **111**, 707 (1958); Y. A. Chang and L. Himmel, J. Appl. Phys. **37**, 3567 (1966).

[8]W. B. Daniels and C. S. Smith, Phys. Rev. **111**, 713 (1958).

[9]D. L. Martin, Phys. Rev. Lett. **12**, 723 (1964); Phys. Rev.

141, 576 (1966); Phys. Rev. **170,** 650 (1968).
[10]M. K. Wilkinson, H. G. Smith, W. C. Koehler, R. M. Nicklow, and R. M. Moon, in *Neutron Inelastic Scattering* (International Atomic Energy Agency, Vienna, 1968), Vol. II, p. 253.
[11]G. F. Koster, in *Solid State Physics*, edited by F. Seitz and D. Turnbull (Academic, New York, 1957), Vol. 5, p. 173.
[12]A. P. Miiller, B. N. Brockhouse, and J. M. Rowe, Phys. Can. **22,** 24 (1966); A. P. Miiller and B. N. Brockhouse, Can. J. Phys. **49,** 704 (1971).
[13]D. H. Dutton, B. N. Brockhouse, and A. P. Miiler, Can. J. Phys. **50,** 2915 (1972); R. Ohrlich and W. Drexel, in Ref. 10, Vol. I, p. 203.
[14]Details of these calculations are given in Refs. 4 and 23.
[15]G. L. Squires, *Inelastic Scattering of Neutrons in Solids and Liquids* (International Atomic Energy Agency, Vienna, 1963), Vol. II, p. 71.
[16]W. A. Harrison, *Pseudopotentials in the Theory of Metals* (Benjamin, New York, 1966).
[17]For recent calculations of the lattice dynamics of the noble metals see, for example, S. Prakash and S. K. Joshi, Phys. Rev. B **5,** 2880 (1972); B. Prasad and R. S. Srivastava, J. Phys. F **2,** 247 (1972); J. A. Moriarty, Phys. Rev. B **6,** 1239 (1972); W. Hanke and H. Bilz, *Neutron Inelastic Scattering* (International Atomic Energy Agency, Vienna, 1972), p. 3; P. K. Sharma and N. Singh, Phys. Rev. B 4, 4636 (1971).
[18]Details of these pseudopotential calculations are given in M. Mostoller, Phys. Rev. B **5,** 1260 (1972), and references therein.
[19]P. J. Lin and L. Kleinman, Phys. Rev. **142,** 478 (1966).
[20]For a recent discussion of the use of pseudopotentials for *d*-electron metals, see P. B. Allen, Phys. Rev. B **6,** 4069 (1972), and references therein.
[21]A comparison of the free-ion sizes of the noble metals with their nearest-neighbor distances indicates that gold should have the most core-core overlap.
[22]G. Gilat and L. J. Raubenheimer, Phys. Rev. **144,** 390 (1966).
[23]G. Gilat and R. M. Nicklow, Phys. Rev. **143,** 487 (1966).
[24]All the third-order elastic constants of the noble metals are negative. Y. Hiki and A. V. Granato, Phys. Rev. **144,** 411 (1966).
[25]T. H. Geballe and W. F. Giauque, J. Am. Chem. Soc. **74,** 2368 (1952).
[26]W. S. Corak, M. P. Garfunkel, C. B. Satterthwaite, and A. Wexler, Phys. Rev. **98,** 1699 (1955).
[27]F. J. du Chatenier and J. de Nobel, Physica (Utr.) **28,** 181 (1962).
[28]See, for example, S. K. Joshi and A. K. Rajagopal, in Ref. 11, Vol. 22, p. 159; A. A. Maradudin, E. W. Montroll, G. H. Weiss, and I. P. Ipatova, *Theory of Lattice Dynamics in the Harmonic Approximation* (Academic, New York, 1971), Chap. 1V; a simple discussion is given by C. Kittel, *Introduction to Solid Space Physics,* 4th ed. (Wiley, New York, 1971), Chap. 6.
[29]R. J. Birgeneau, J. Cordes, G. Dolling, and A. D. B. Woods, Phys. Rev. **136,** A1359 (1964).
[30]R. M. Nicklow, (unpublished).
[31]W. T. Berg, Phys. Rev. **167,** 583 (1968). A discussion of the relation between $g(\nu)$ and an initial rise in $\Theta_C(T)$ along with references to earlier literature, is given here.
[32]D. J. Erickson, L. D. Roberts, J. W. Burton, and J. O. Thomson, Phys. Rev. B **3,** 2180 (1971).
[33]A table of values is given in E. F. Skelton and J. L. Feldman, Acta Crystallogr. A **27,** 484 (1971).